Optics Letters

# Self-referenced temperature sensing with a lithium niobate microdisk resonator

Rui Luo,[1] Haowei Jiang,[1,2,3] Hanxiao Liang,[2] Yuping Chen,[3] and Qiang Lin[1,2,*]

[1]Institute of Optics, University of Rochester, Rochester, New York 14627, USA
[2]Department of Electrical and Computer Engineering, University of Rochester, Rochester, New York 14627, USA
[3]Department of Physics and Astronomy, Shanghai Jiao Tong University, Shanghai 200240, China
*Corresponding author: qiang.lin@rochester.edu

Received 12 January 2017; revised 17 February 2017; accepted 17 February 2017; posted 21 February 2017 (Doc. ID 284481); published 23 March 2017

**Self-referenced temperature sensing based on thermo-optic birefringence is demonstrated on a Z-cut lithium niobate microdisk resonator. Due to the significant difference between thermo-optic coefficients of ordinary and extraordinary light, quasi-transverse magnetic (quasi-TM) and quasi-transverse electric (quasi-TE) modes in the microdisk show relative cavity resonance shift upon temperature change, which acts as a robust self-reference for temperature sensing. A temperature sensitivity of 0.834 GHz/K and a measurement uncertainty of 0.8 mK are demonstrated with an optical input power of only 1.5 μW.** 

***OCIS codes:*** (130.3730) Lithium niobate; (120.6780) Temperature.

https://doi.org/10.1364/OL.42.001281

Photonic microresonators with narrow-linewidth cavity resonances are widely employed for many sensing applications [1,2]. Due to the thermo-refraction and/or thermo-expansion, a resonance frequency of a high-$Q$ resonator generally depends sensitively on device temperature. This simple mechanism can be applied to temperature sensing, which has been demonstrated on a variety of device and material platforms, from polymer and silica microspheres [3–6], silica microtoroids [7], silica microbubbles [8], and liquid microspheres [9], to silicon microring resonators [10,11]. As this approach relies on the direct mapping of the temperature from cavity resonance wavelength, its practical implementation would require external wavelength calibration for proper operation.

An alternative approach is to utilize the differential frequency shift (DFS) between two cavity resonances induced by temperature variation [12]. This approach is based on frequency separation between two cavity resonances which does not require calibration of individual cavity resonances, thus forming an elegant method for *self-referenced* temperature sensing. The dispersion and the birefringence of thermo-refractivity, which introduce temperature-dependent DFS between two-color cavity resonances [13,14] and two polarization modes [12,15], respectively, can both be employed for this purpose. The dispersion of thermo-refractivity is generally fairly small, which requires either far separate two-color resonances (e.g., fundamental and second harmonic [14]) or a second mechanism (e.g., optomechanics [13]) to enhance the sensing signal. Thermo-optic birefringence, in contrast, is usually quite significant for crystalline media [16] and, thus, offers a convenient and flexible approach for self-referenced temperature sensing, which has been demonstrated recently in $MgF_2$ and $CaF_2$ resonators [15,17,18].

In this Letter, we demonstrate self-referenced temperature sensing in an on-chip lithium niobate (LN) high-$Q$ microresonator, by taking advantage of its strong thermo-optic birefringence. The device exhibits a significant temperature sensitivity of 0.834 GHz/K, about one order of magnitude larger than other self-referenced sensing device platforms [15,17,18], which allows us to measure a temperature uncertainty of 0.8 mK with an optical power of only 1.5 μW. In contrast to other devices [15,17,18], the on-chip platform of the demonstrated device exhibits great potential for chip-scale integration for future practical implementation.

Congruent single-crystalline lithium niobate exhibits strong birefringence on its thermo-optic coefficients, whose values at the telecom band are given as [19]

$$\frac{dn_o}{dT} = (0.9 + 3 \times 10^{-3} T) \times 10^{-5}\ \mathrm{K}^{-1}, \tag{1}$$

$$\frac{dn_e}{dT} = (-2.6 + 19.8 \times 10^{-3} T) \times 10^{-5}\ \mathrm{K}^{-1}, \tag{2}$$

where $T$ is the temperature in Kelvin, and $n_o$ and $n_e$ are the refractive indices for the ordinary and extraordinary light, respectively. On the other hand, it also exhibits orientation-dependent thermo-expansion coefficients [20]:

$$\alpha_l^{(X,Y)} = (1.22 + 1.06 \times 10^{-3} T) \times 10^{-5}\ \mathrm{K}^{-1}, \tag{3}$$

$$\alpha_l^{(Z)} = (1.21 - 1.54 \times 10^{-3} T) \times 10^{-5}\ \mathrm{K}^{-1}, \tag{4}$$

where $\alpha_l^{(X,Y)}$ and $\alpha_l^{(Z)}$ are the linear thermo-expansion coefficients along the directions perpendicular and parallel to the optical axis, respectively. The strong thermo-optic birefringence of LN implies its great potential for self-referenced temperature sensing. This is particularly enabled by recent advances in the nanofabrication of LN photonic devices, which produce

high-$Q$ LN microresonators available on a chip-scale platform [21–24].

The device we employed is a LN microdisk resonator fabricated on a Z-cut LN-on-insulator wafer, with a radius of 25 μm and a thickness of 400 nm, sitting on a 2 μm thick silica pedestal [Fig. 1, insets, and Fig. 2(b)]. The device exhibits quasi-transverse electric (quasi-TE) and quasi-transverse magnetic (quasi-TM) cavity modes, with electric fields dominantly in parallel and perpendicular to the device plane, respectively (Fig. 1, insets). For a Z-cut LN microdisk, the optical axis aligns normally to the device plane. As a result, a quasi-TE and a quasi-TM cavity mode primarily correspond to an ordinary and an extraordinary polarization of the LN crystal, respectively (Fig. 1, insets), resulting in maximal thermo-optic birefringence between them, which is ideal for self-referenced temperature sensing. For example, Eqs. (1) and (2) show that, at room temperature, the thermo-optic coefficient is nearly zero for the ordinary polarization ($\frac{dn_o}{dT} \approx 0$) at a telecom-band wavelength, while it is fairly significant for the extraordinary polarization ($\frac{dn_e}{dT} \approx 3.34 \times 10^{-5}$/K).

To explore the sensing potential of our device, we performed numeric modeling of the thermo-optic properties of the cavity resonances, including both thermo-refraction and thermo-expansion effects, simulated by the finite element method. Figure 1 shows the simulated temperature-dependent cavity resonance frequencies, $f_{\mathrm{TE}}$ and $f_{\mathrm{TM}}$, of the fundamental quasi-TE ($\mathrm{TE}_0$) mode (red curve) and the fundamental quasi-TM ($\mathrm{TM}_0$) mode (blue curve) at the telecom-band, respectively. In general, both resonance frequencies shift toward red with increased device temperature because of the combined effect of thermo-refraction and thermo-expansion. However, due to the significantly larger thermo-refractivity of the extraordinary light, the quasi-TM mode shifts by a larger amount, and the frequency separation between the two modes, $\Delta f \equiv f_{\mathrm{TM}} - f_{\mathrm{TE}}$, depends sensitively on temperature (black curve), resulting in a considerable DFS with a significant tuning slope of $\frac{d\Delta f}{dT} = -1.019$ GHz/K. This implies that 1 mK drift of the device temperature would result in a DFS of about 1 MHz, which can be conveniently resolved by a high-$Q$ microresonator with a reasonable signal-to-noise ratio (SNR), as will be shown in the following paragraphs of this Letter.

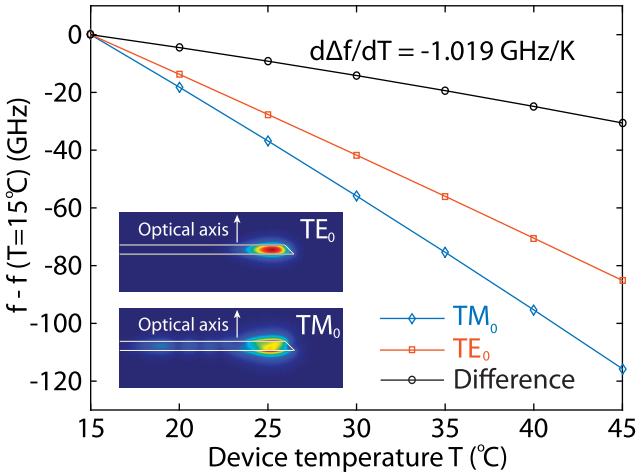


**Fig. 1.** Temperature dependence of resonance frequencies of the fundamental quasi-TM mode (blue) and the fundamental quasi-TE mode (red) for a Z-cut LN microdisk resonator, simulated by the finite element method. For easy illustration, the resonance frequencies are plotted in reference to those at 15°C. The black curve shows the frequency difference between the two cavity modes. The device has a radius of 25 μm, a thickness of 400 nm, and a slant angle of 45° on the disk sidewall [which is introduced by a device etching process. See Fig. 2(b)]. Symbols are simulation results, and solid lines are linear fittings. The quasi-TM and quasi-TE modes have azimuthal mode numbers of 151 and 189, respectively, with resonance wavelengths both close to 1500 nm. The insets show the electric field profiles of the two cavity modes.

To demonstrate the proposed self-referenced temperature sensing, we conducted experiments with the setup shown in Fig. 2(a). The temperature of the LN device is controlled by a thermoelectric cooler. The set temperature is stabilized by a temperature controller (Newport 350B, with a short-term stability of 1 mK). The device operates in the atmospheric environment. A continuous-wave tunable diode laser (New Focus 6326) is launched into the device via evanescent coupling with a tapered optical fiber, to probe the induced DFS between a quasi-TE and a quasi-TM cavity mode.

We selected a quasi-TE and a quasi-TM cavity resonance in the telecom band around 1502 nm, with resonance frequencies close to each other such that both cavity resonances lie in the laser fine tuning range. Figure 3(a) shows the laser-scanned transmission spectra of the two cavity resonances. The quasi-TE and quasi-TM modes are both undercoupled and exhibit loaded optical Q's of $2.9 \times 10^5$ and $2 \times 10^5$, respectively, corresponding to cavity linewidths of 0.7 and 1 GHz. At 30°C, the quasi-TM mode has a higher frequency, 18 GHz separated from that of the quasi-TE mode. When the device temperature increases, the two cavity resonances, $f_{\mathrm{TM}}$ and $f_{\mathrm{TE}}$, shift toward red (not shown in Fig. 3). However, their frequency separation, $\Delta f = f_{\mathrm{TM}} - f_{\mathrm{TE}}$, decreases until they cross over each other [Fig. 3(b)]. Figure 4(a) shows the recorded temperature dependence of $\Delta f$. As expected, $\Delta f$ decreases linearly with increased temperature until ~45°C, above which the coupling between the

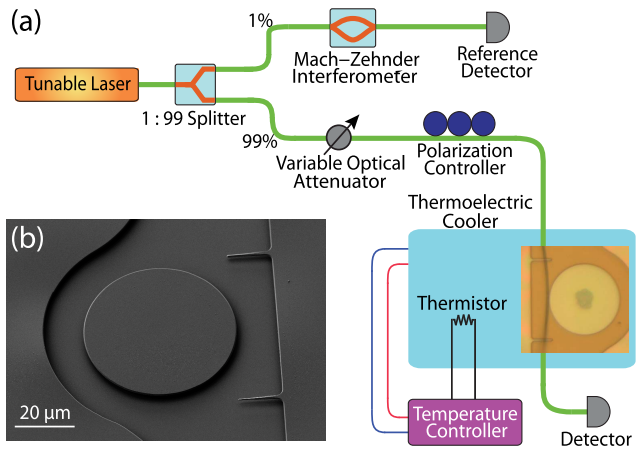


**Fig. 2.** (a) Schematic of our experimental setup. Light from a tunable laser is split into two parts, with a small portion going into a fiber Mach–Zehnder interferometer as a reference, and a large portion coupled to the LN microdisk via a fiber taper. The device chip is placed on a thermoelectric cooler whose temperature is stabilized by a temperature controller. (b) Scanning electron microscope image of a typical fabricated LN microdisk.

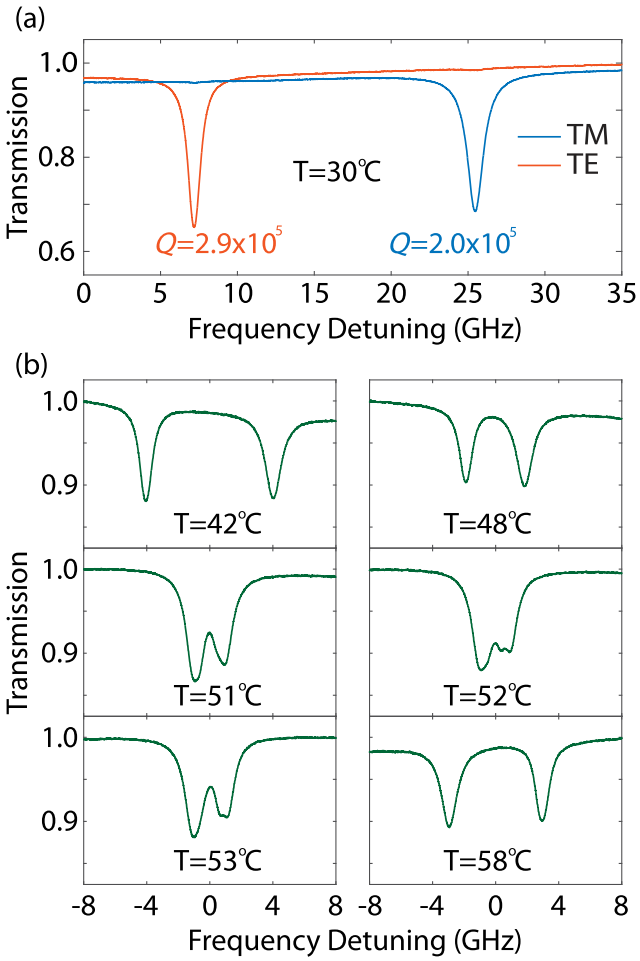


**Fig. 3.** (a) Transmission spectra of two orthogonal polarizations, showing a quasi-TE (red) and a quasi-TM (blue) resonance. The wavelengths of the two modes are around 1502 nm, and the measurement is made at a temperature of 30°C. (b) Transmission spectra at different temperatures. The polarization of the input light is set such that the two modes have similar coupling depths.

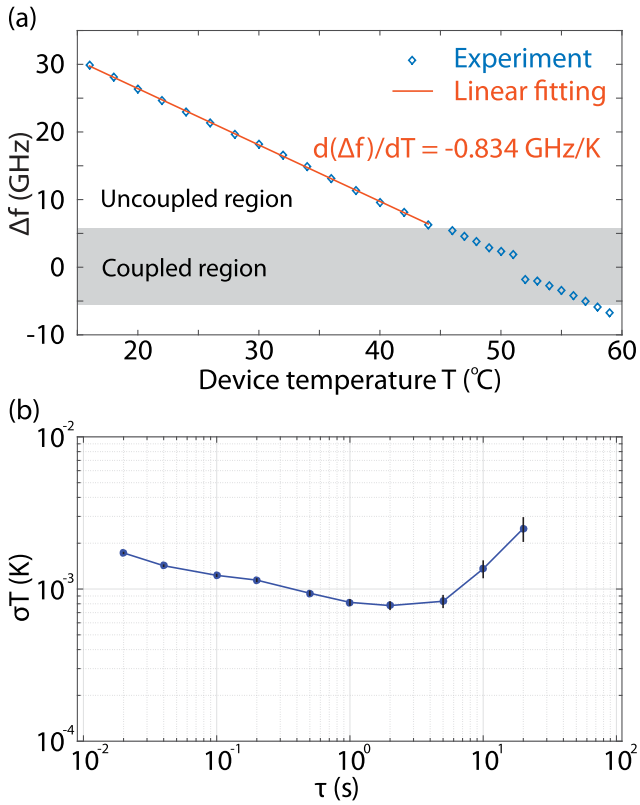


**Fig. 4.** (a) Experimentally recorded frequency difference between the two modes, $\Delta f$, as a function of temperature. The linear curve is fitted from data in the uncoupled region ($T = 16 \sim 44$°C). (b) Allan deviation of temperature measurements at 30°C.

two modes introduces nonlinear temperature dependence of $\Delta f$. In the linear regime, where the sensor will operate, the device exhibits a temperature sensitivity of $\frac{d\Delta f}{dT} = -0.834$ GHz/K, which agrees closely with the theoretical expectation shown in Fig. 1. The experimentally recorded $\frac{d\Delta f}{dT}$ is about one order of magnitude larger than other self-referenced devices [14,15,17,18], implying the great potential of LN devices for self-referenced temperature sensing.

To characterize the sensing resolution, we set the device temperature at 30°C and launched an optical power of 1.5 μW into the LN device to continuously monitor the time-dependent variation of the frequency difference between the two cavity resonances. The optical power is high enough to achieve a large enough SNR at the optical detection of cavity transmission, while low enough to induce negligible nonlinear optical effects. We carried out a repeated measurement at a frequency of 50 Hz and recorded 32768 continuous measurements of $\Delta f$. Figure 4(b) shows the Allan deviation of the detected temperature as a function of the measurement time. The Allan deviation decreases monotonically with increased measurement time, until reaching a minimum value of 0.8 mK at an averaging time of 2 s. This measurement uncertainty directly corresponds to the short-term stability (~1 mK) of our temperature controller employed to stabilize the device temperature. Therefore, the device allows us to probe the minimum temperature uncertainty offered by our current temperature stabilization system.

In principle, the device is expected to offer a sensing resolution considerably higher than this value. The fundamental temperature fluctuation of a microresonator is given by $\langle \mu^2 \rangle = \frac{\kappa T^2}{CV\rho}$ [25], where $\kappa$ is the Boltzmann constant, $C$ and $\rho$ are the specific heat capacity and the density of the device material, and $V$ is the volume of the device. For our LN microdisk resonator, the fundamental temperature fluctuation is estimated to be $\sqrt{\langle \mu^2 \rangle} \approx 23$ μK. The laser frequency noise is expected to play a minor role for the level of optical $Q$ in our device [11]. The impact of the laser intensity noise can be easily eliminated, since it can be normalized by a direct monitoring of the laser power. Therefore, we estimate that the sensing resolution of our device should be considerably better than 0.8 mK. The exact characterization of the sensing resolution will require a better temperature stabilization system, which will be left for future exploration.

In conclusion, we have demonstrated self-referenced temperature sensing with an on-chip Z-cut LN microdisk resonator, based on strong thermo-optic birefringence of LN crystalline material. The device exhibits a temperature sensitivity of

0.834 GHz/K, which allowed us to measure a temperature uncertainty of 0.8 mK with an optical input power of only 1.5 μW. Our device shows great potential for a self-referenced integrated photonic temperature sensor with high sensitivity, high precision, and low power consumption.

**Funding.** National Science Foundation (NSF) (ECCS-1509749, ECCS-1610674); Shanghai Jiao Tong University (SJTU) (2016GZKF0JT001).

**Acknowledgment.** The authors thank Wei C. Jiang for helpful discussions. This Letter was performed in part at the Cornell NanoScale Science and Technology Facility (CNF), a member of the National Nanotechnology Infrastructure Network.

## REFERENCES

1. X. Fan, I. M. White, S. I. Shopova, H. Zhu, J. D. Suter, and Y. Sun, Anal. Chim. Acta **620**, 8 (2008).
2. M. R. Foreman, J. D. Swaim, and F. Vollmer, Adv. Opt. Photon. **7**, 168 (2015).
3. C.-H. Dong, L. He, Y.-F. Xiao, V. R. Gaddam, S. K. Ozdemir, Z.-F. Han, G.-C. Guo, and L. Yang, Appl. Phys. Lett. **94**, 231119 (2009).
4. Q. Ma, T. Rossmann, and Z. Guo, Meas. Sci. Technol. **21**, 025310 (2010).
5. Y.-Z. Yan, C.-L. Zou, S.-B. Yan, F.-W. Sun, Z. Ji, J. Liu, Y.-G. Zhang, L. Wang, C.-Y. Xue, W.-D. Zhang, Z.-F. Han, and J.-J. Xiong, Opt. Express **19**, 5753 (2011).
6. L. L. Martin, C. Perez-Rodriguez, P. Haro-Gonzalez, and I. R. Martin, Opt. Express **19**, 25792 (2011).
7. B.-B. Li, Q.-Y. Wang, Y.-F. Xiao, X.-F. Jiang, Y. Li, L. Xiao, and Q. Gong, Appl. Phys. Lett. **96**, 251109 (2010).
8. J. M. Ward, Y. Yang, and S. N. Chormaic, IEEE Photon. Technol. Lett. **25**, 2350 (2013).
9. Z. Liu, L. Liu, Z. Zhu, Y. Zhang, Y. Wei, X. Zhang, E. Zhao, Y. Zhang, J. Yang, and L. Yuan, Opt. Lett. **41**, 4649 (2016).
10. G.-D. Kim, H.-S. Lee, C.-H. Park, S.-S. Lee, B. T. Lim, H. K. Bae, and W.-G. Lee, Opt. Express **18**, 22215 (2010).
11. H. Xu, M. Hafezi, J. Fan, J. M. Taylor, G. F. Strouse, and Z. Ahmed, Opt. Express **22**, 3098 (2014).
12. A. A. Savchenkov, A. B. Matsko, V. S. Ilchenko, N. Yu, and L. Maleki, J. Opt. Soc. Am. B **24**, 2988 (2007).
13. A. B. Matsko, A. A. Savchenko, V. S. Ilchenko, D. Seidel, and L. Maleki, Phys. Rev. A **83**, 021801 (2011).
14. W. Weng, J. D. Anstie, T. M. Stace, G. Campbell, F. N. Baynes, and A. N. Luiten, Phys. Rev. Lett. **112**, 160801 (2014).
15. D. V. Strekalov, R. J. Thompson, L. M. Baumgartel, I. S. Grudinin, and N. Yu, Opt. Express **19**, 14495 (2011).
16. W. J. Tropf, M. E. Thomas, and T. J. Harris, *Handbook of Optics*, M. Bass, E. W. V. Stryland, D. R. Williams, and W. L. Wolfe, eds., 2nd ed. (McGraw-Hill, 1995), Vol. **2**, pp. 33.1–33.100.
17. I. Fescenko, J. Alnis, A. Schliesser, C. Y. Wang, T. J. Kippenberg, and T. W. Hänsch, Opt. Express **20**, 19185 (2012).
18. L. M. Baumgartel, R. J. Thompson, and N. Yu, Opt. Express **20**, 29798 (2012).
19. L. Moretti, M. Lodice, F. G. D. Corte, and I. Rendina, J. Appl. Phys. **98**, 036101 (2005).
20. Y. S. Kim and R. T. Smith, J. Appl. Phys. **40**, 4637 (1969).
21. C. Wang, M. J. Burek, Z. Lin, H. A. Atikian, V. Venkataraman, I.-C. Huang, P. Stark, and M. Lončar, Opt. Express **22**, 30924 (2014).
22. J. Lin, Y. Xu, Z. Fang, M. Wang, J. Song, N. Wang, L. Qiao, W. Fang, and Y. Cheng, Sci. Rep. **5**, 8072 (2015).
23. J. Wang, F. Bo, S. Wan, W. Li, F. Gao, J. Li, G. Zhang, and J. Xu, Opt. Express **23**, 23072 (2015).
24. W. C. Jiang and Q. Lin, Sci. Rep. **6**, 36920 (2016).
25. M. L. Gorodetsky and I. S. Grudinin, J. Opt. Soc. Am. B **21**, 697 (2004).